PET vs. SPECT: in the Context of Ongoing Developments (Review Article)

Arman Rahmim, PhD

Department of Radiology, School of Medicine,

Johns Hopkins University, Baltimore MD, USA

ABSTRACT

This paper intends to compare the abilities of the two major imaging modalities in nuclear medicine imaging: Positron Emission Tomography (PET) and Single Photon Emission Computed Tomography (SPECT). The motivations are many-fold:

(i) To gain a better understanding of the strengths and limitations of the two imaging modalities in the context of recent and ongoing developments in hardware and software design;

(ii) To emphasize that certain issues, historically and commonly thought as limitations, may now be instead viewed as challenges that can be addressed;

(iii) To point out that existing PET and SPECT scanners in the field can (much) benefit from improvements in image-reconstruction software;

(iii) To point-out (to engineers, physicists and software-developers) important areas of research in PET and SPECT imaging that will be instrumental to further improvements in the two modalities;

Key Words: *PET, SPECT, Sensitivity, Spatial resolution, Temporal resolution, Dynamic imaging, Attenuation, Collimator, Random coincidence, Animal imaging, Dual isotope imaging, Time-of-Flight*

Corresponding author: Arman Rahmim PhD, Division of Nuclear Medicine, Department of Radiology, School of Medicine, Johns Hopkins University, Baltimore MD 21287, USA

E-mail:arahmim1@jhmi.edu

I. INTRODUCTION

This paper intends to compare, in the context of recent and ongoing developments, the abilities of the two major imaging modalities in nuclear medicine imaging: Positron Emission Tomography (PET) and Single Photon Emission Computed Tomography (SPECT). Comparison of the two imaging modalities in terms of the *biology* needs to be presented elsewhere, and except for very brief comments, this review focuses on the *physics* of imaging (hardware and software). At first glance, it may be thought that the targeting abilities (and therefore *biological* aspects) of different compounds in PET vs. SPECT are the *only* issues to consider in order to select which to use in each context[1]. However, such an isolated approach, in which physical abilities of the two scanners are neglected, is bound to result in (costly) mistakes and problems.

The importance of physical considerations can be better seen, for example, in the case of cardiac PET vs. SPECT. Coronary perfusion and myocardial viability are most commonly performed with SPECT scanners[2]. At the same time, some data suggest that PET may offer increased accuracy compared to SPECT (2), particularly for heavier patients, where breast,

chest wall, and diaphragmatic attenuation interfere with conventional SPECT. This is because attenuation correction is easily achieved in PET, whereas it is (often) not implemented accurately in SPECT. However, latest trends in SPECT imaging attempt to accurately address attenuation correction (see Sec. V), and therefore the latest generation of SPECT cameras (or improved software for current SPECT cameras) should be able to produce increased accuracy.

In this work, sections II, III and IV compare capabilities in PET and SPECT in terms of sensitivity, spatial resolution and temporal resolution, respectively. Various ongoing developments enhancing performance of PET and SPECT are discussed, both in terms of hardware (e.g. slant-hole and pinhole collimators) and software (e.g. finite resolution modeling, dynamic image reconstruction). Complications related to attenuation correction (especially in SPECT) and random-coincidences (in PET) are explained in sections V and VI. Finally, time-of-flight detection (unique to PET) and dual-isotope imaging (unique to SPECT) are emphasized in sections VII and VIII as additional areas of research and improvement. Other corrections (scatter, partial volume and motion corrections) necessary for obtaining quantitatively accurate images are discussed in Sec. IX. Concluding remarks are presented in Sec. X.

II. SENSITIVITY

The most important advantage of PET imaging over SPECT is that of exhibiting a much higher sensitivity (by ~2-3 orders of magnitude): i.e. the ability to detect and record a higher percentage of the emitted events, which has very important implications (described in Sec. II-B). This is because, in single photon imaging (planar gamma imaging and SPECT), collimators are

---

1. Certainly, biological considerations are the *ultimate* deciding factors when comparing PET vs. SPECT. It is also worth noting that in the biological context, generalized comparisons are not appropriate; instead they need to be performed on a case-by-case basis. For instance, it is often said that natural occurrence of PET isotopes in biologically active molecules (as opposed to heavy isotopes used in SPECT) results in a less challenging task of synthesizing physiologically useful tracers in PET (1). On the other hand, in some applications, SPECT agents can provide more specific targeting abilities than PET agents.

2. While SPECT has applications in neurology and oncology, majority of SPECT scans are in cardiology. SPECT is now a cornerstone with any patient with heart disease.

needed in order to reject photons that are not within a small angular range (or else angle of incidence will not be known). Collimators therefore exhibit limited geometric efficiencies (defined as the percentage of detected to emitted photon), of the order of 0.01%.

A) SPECT Collimators

In SPECT, a number of collimator-based approaches to increasing sensitivity are possible. One approach is to use shorter collimators in order to reject a smaller portion of incident events; however, this approach degrades the resolution of the scanner (sensitivity vs. resolution trade-off). On the other hand, novel types of collimators (as opposed to conventional parallel-hole collimators) have been able to improve sensitivity without adversely affecting resolution[3]. Important examples of these include (i) rotating slat collimators (3), (ii) converging-hole (e.g. fan-beam and cone-beam) collimators (4), and (iii) rotating multi-segment slant-hole (RMSSH) collimators (5). The first method uses the idea of rotating parallel slats, with the intrinsic advantage of slats (instead of holes) having a much larger solid angle of acceptance. The second and third methods, instead, gain in sensitivity by means of scanning a smaller field-of-view (FoV).

Particularly interesting are RMSSH collimators (shown in Fig. 1) because in addition to improving the scanner sensitivity by a factor of ~2 or ~4 (depending on whether 2 or 4 segments are used), they can achieve complete angle tomography, with as few as $180o/(2S)$ camera positions where σ is the slant angle (e.g. only 3

camera positions when $S = 30^0$. which corresponds to a single camera stop for a triple-head scanner, assuming sufficient collimator rotation-sampling is performed at the camera positions (see (5,6)). Furthermore, the amount of camera rotation needed is 180o-2S (i.e. less than 180°) making it very convenient for SPECT mammography since the camera can be placed closer to the breast (making it suitable for detecting small, low-contrast breast legions). This is also shown in Fig. 1.
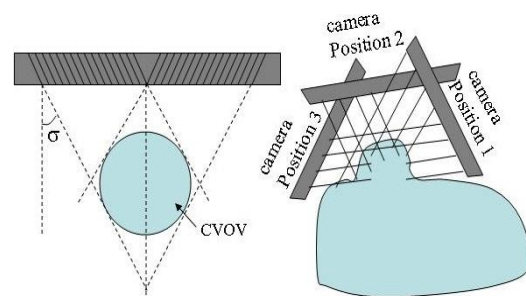

Figure 1: (left) A 2-segment slant-hole collimator. Parallel holes within each segment are slanted towards a common-volume-of-view (CVOV) where the organ to be imaged is placed. The slant-angle S. is shown. (right) Three camera stops, equally spaced around the organ (for $S = 30^o$, only 120° needs to be covered), while the collimator rotates at each camera stop.

B) Coincidence Detection in PET

Due to the nature of positron annihilation in which two opposite gamma rays are emitted from the same event, physical collimators can be entirely removed in PET, with the collimation instead performed electronically using the coincidence-detection method (see Fig. 2). This implies a much larger angle of acceptance at each detector position, resulting in the order of ~1% of emitted events being detected in PET.

---

3. It must be noted that the task of tomography is performed differently for each collimators design, and therefore specifically designed reconstruction algorithms need to be implemented.
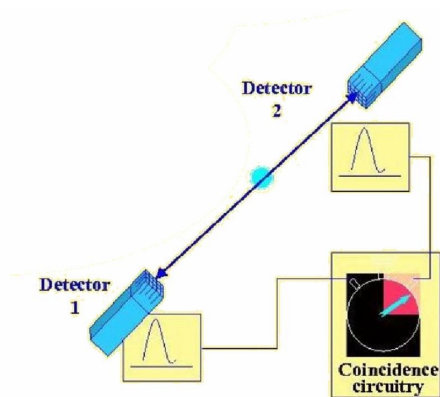
Figure 2: In PET imaging systems, coincidence detection is used, in which two events arriving within a certain coincidence time window are used to trace the path along which the annihilation occurred.

There are a number of important implications to this significant gain in sensitivity for PET:

(1) Improved image quality: primarily due to the random (Poisson) nature of radioactive emissions, noise is an inherent component of nuclear medicine imaging. For multiple measurements, the percentage noise (ratio of standard-deviation σ to average μ of total-counts detected in a certain time interval) along a projection is given by:

$$\% \text{ noise} = \frac{s}{m} = \frac{1}{\sqrt{m}} \qquad (1)$$

because $s = \sqrt{m}$ in Poison statistics. Improvements in sensitivity (i.e. increasing μ) therefore improve signal-to-noise ratios (SNRs) in the data, which also corresponds to improvements in image SNRs (see (7,8,9) for details of methods relating data SNRs to image SNRs).

(2) Possibility of performing shorter scans: an increase in sensitivity implies the ability to acquire shorter scans with similar SNRs.

(3) Multiple field-of-view (FoV) scanning: the ability to perform shorter scans also implies the feasibility of performing multiple scans of a patient at different fields-of-views in a reasonable time. This is a very important consideration in diagnostic oncology.

(4) Improved temporal resolution: as will be elaborated in Sec. IV, higher sensitivity of PET scanners implies an increased ability to acquire shorter (and therefore higher number of) frames in dynamic studies, resulting in an improved ability to study image dynamics.

It must be noted that the technique of coincidence-detection used in PET, while highly improving sensitivity, introduces two issues which have been subjects of further investigation:

(1) Photon non-collinearity effect (see Sec. III-C).

(2) Detection of random coincidences (see Sec. VI);

C) Effect of Short Half-Lives in PET

In the present context, an additional observation is that the short half-lives of radionuclides used in PET effectively allow for increased detection sensitivity over a given period of time. This is because compared to SPECT imaging, radiotracers with shorter half-lives can be injected in higher activities to the patient without posing any additional radiation damage to the patient (because overall accumulation over time remains the same) thus generating increased detectable radiation over a smaller time.

An example of this, with much recent interest, is rubidium(Rb)-based PET. Because rubidium has a very short physical half-life of only 76 seconds, it can be injected in very high (yet safe) amounts (e.g. 50mCi) allowing for acceptable images in very short times. Compared to routine SPECT myocardial stress imaging, which can take place

over three to four hours[4], a complete pharmacological stress-and-rest test may instead be performed in well under an hour in Rb-based cardiac PET (considerably increasing patient comfort as well as number of daily patient scans). In addition, the almost-instantaneous ability of rubidium to image a patient has provided a very high accuracy in identification of ischemia (10).

III. SPATIAL RESOLUTION

Spatial resolution in PET and SPECT is related to a number of different factors. A general observation is that improvements in SPECT resolution are effectively only limited by technology (e.g. collimator design), whereas in PET imaging, two physics-related limitations, namely positron range and photon non-collinearity, ultimately limit system resolution (it must however be noted that, as discussed later, these effects can be modeled in the reconstruction task, as opposed to simply being treated as resolution-limiting, therefore further improving reconstructed resolutions). We discuss related issues next.

A) Pinhole SPECT

Pinhole SPECT is an exciting example of technological advance which has introduced the possibility of considerably enhancing image resolution in SPECT (to sub-millimeter scale), particularly in the context of small animal imaging (e.g. see (11) with additional references). However, it must be noted that use of a small pinhole further decreases system sensitivity. Subsequently, multi-pinhole collimators have been proposed and implemented (12), an example of which mounted

---

4. This time can be potentially halved using simultaneous dual-isotope imaging as elaborated in Sec. VIII.

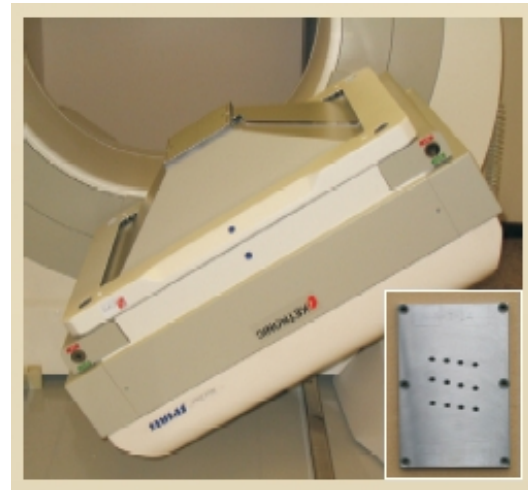on a standard clinical SPECT camera is shown in Fig. 3.

Figure 3: Example of a multi-pinhole collimator mounted on a clinical gamma camera.

A complicating factor with the high-resolution pinhole approach is the task of calibrating the SPECT devices (especially in the presence of camera rotations). An innovative solution to this consideration, which at the same time noticeably increases system sensitivity, is the design of stationary dedicated pinhole SPECT systems making use of a large number of compact detectors with multiple pinhole geometries. An example of such design is the U-SPECT-III system (13) containing 135 pinholes, as shown in Fig. 4. Therefore, stationary multi-pinhole SPECT imaging using dedicated detectors provides a combination (and not trade-off) of high-resolution and high-sensitivity, and furthermore, considerably enhances possibilities of dynamic imaging. However, one may add that these systems would still likely require axial translation schemes since they cover a very limited field-of-view (FoV).
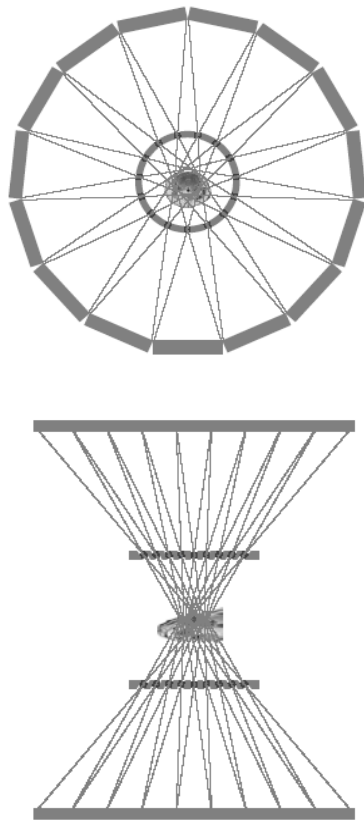
Figure 4: The design of U-SPECT-III contains a total of 135 gold pinhole apertures: 15 pinholes in each ring (top) with a total of 9 rings (bottom). Not shown here is that pinhole positions in adjacent rings are rotated transaxially with respect to each other by 8o in order to increase the variety of angles at which each voxel is observed.

B) Finite Resolution Effects in SPECT

In SPECT, the image generated from a point-source is degraded by a number of factors related to collimators and detectors in gamma cameras, thus referred to as the collimator-detector response (CDR). Therefore, for any particular SPECT scanner, the CDR can be a measure of the image resolution; however, this is only if no further compensation is included. In recent years, a great deal of work has gone into developing methods to compensate for the CDR.

The CDR is determined by the following four factors:

(1) Intrinsic Response: Aside from the effect of collimators, the detector system itself demonstrates an intrinsic uncertainty in position estimation of incident gamma rays. This is caused by two factors: (a) the statistical signal variation (noise) in signal output of PMTs used for position estimation, and (b) change/spread in signal energy deposition in the detector due to scattering (especially for higher energy isotopes e.g. In-111).

(2) Geometric Response: Collimators dimensions define the acceptance angle within which incident photons are accepted. Subsequently, the geometric response function becomes wider with increasing distance from the collimator surface, and strongly depends on the particular design of each collimator.

(3) Septal Penetration: The CDR is further degraded due to the penetration of some photons through the collimator septa. No analytic treatment of this effect appears to exist in the literature, and Monte Carlo (MC) simulation techniques have instead been used (e.g. (14)).

(4) Septal Scatter: This effect is caused by photons that scatter in the collimator septa and still remain within the detection energy window. Similar to septal penetration, this effect may also be computed using MC simulation techniques.

Analytic methods taking into account the distance-dependence of the CDR function (CDRF) have been proposed in the literature (see (15) for a review of both related analytic and statistical methods). However, compared to statistical methods, such analytic methods suffer from (i) a general lack of ability to treat statistical noise in the data, and (ii) making specific approximations, for instance with regards to the shape and/or distance-dependence of the CDRF, in order to arrive at analytic solutions.

With the increasing realization of the power of

statistical methods in nuclear medicine, and particularly with the development of convenient and fast rotation-based projectors in SPECT (16,17), as shown in figure 5, iterative reconstruction methods incorporating distant-dependent CDRFs are increasing in popularity[5].
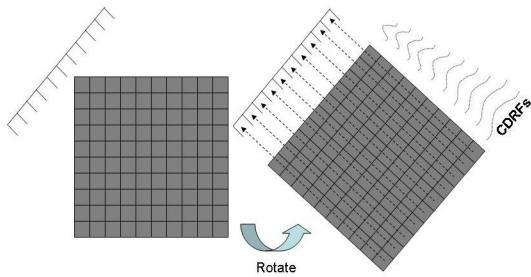

Figure 5: Rotation-based projector methods incorporating distant-dependent CDRFs make use of the fact that, for parallel-beam deometries, the CDRF is spatially invariant in rows (planes) parallel to the collimator face. Thus, each row (plane) may be convolved with the appropriate distance-dependent CDRF.

Incorporation of CDR modeling in reconstruction algorithms (especially statistical methods) has been shown to result in improvements in resolution (18), noise (20), and more importantly in task-based measures of image-quality: e.g. improved uniformity in the myocardial wall as well as improved estimates of wall thickness (21), improved observer myocardial defect detection in both simulated (22,23) and clinical (24) data, as well as improved performance for tumor detection and localization (25).

C) Finite Resolution Effects in PET

In PET imaging, three factors contribute to degradation of resolution in the reconstructed images: detector-related effects, photon non-collinearity and positron range. Detector-related effects (which in PET are due to (i) the width of crystal scintillators, (ii) inter-crystal scattering, and (iii) Inter-crystal penetration) are continually improving with advances in technology, and similar to CDR compensation in SPECT, may be modeled in the reconstruction task (e.g. see (26)) to further improve reconstructed resolutions. In what follows, we elaborate the remaining two inherent resolution-degrading factors in PET:

Photon non-collinearity: Since the net momentum for an emitted positron, and the electron with which it annihilates, can be non-zero, this results in deviations from 180o between the trajectories of the two emitted photons (due to conservation of momentum) as shown in Fig. 6. This deviation is around 0.25o FWHM, and the corresponding resolution blurring depends on detector separation D, and is approximately given by

$$FWHM \approx \left(0.25 \times \frac{p}{180} \right) \frac{D}{2} \qquad (2)$$

That is:

$$FWHM \approx 0.0022 \times D \qquad (3)$$

Therefore one expects ~1.1 mm FWHM blurring for a typical whole-body scanners (D~0.5 m), whereas this blurring may be much reduced for animal scanners (e.g. only 0.17 mm for D~8 cm).

---

5. Use of Gaussian diffusion methods (18,19) can further increase the speed of rotation-based projectors.
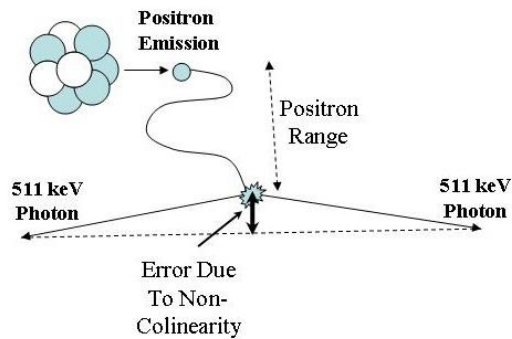
Figure 6: Depiction of photon non-collinearity and positron range effects in the positron annihilation process.

Positron range: Emitted positrons are required to travel a certain distance, on the average, in the surrounding medium before they can reach thermal energies in order to be annihilated: this distance is referred to as the positron range (shown in Fig. 6). Different positron-emitting isotopes exhibit distinct energy distributions, and therefore also exhibit different positron range values. See (27) for an extensive analysis of positron range distributions.

Traditionally, positron range has been viewed as purely resolution-limiting. However, there are two additional approaches (one hardware-based and the other software based) that can be used to reduce this effect:

(1) Application of a magnetic field: Simulations (28,29) as well as experiments (29) have verified the possibility of improving PET scanner resolution by application of a magnetic field, which is known to reduce the positron range. This is a possible advantage of PET systems compatible with MRI/NMR systems[6]. It must be

noted that this effect is most significant: (i) at field strengths of ~5 Tesla or more; (ii) for high-energy positrons-emitting radionuclides e.g. Ga-68 and Rb-82.

However, when employing lower-energy positron-emitting radionuclides such as F-18 or C-11, simulations/experiments with typical human PET scanners (resolutions of ~3 mm or more) have indicated (28,29) that improvements in resolution will not to be significant. For such radionuclides, this effect may only become noticeable for small animal scanners (and remains to be demonstrated): this is because, in addition to having smaller detectors, effect of photon non-collinearity is also small in animal PET scanners (see Eq. 3), and therefore reductions in positron range will more readily affect overall scanner resolution.

(2) Modeling into the reconstruction task: Positron range (and photon non-collinearity) are conventionally not discussed as physical phenomenon that can be corrected for, rather they are often seen as limitations of PET imaging. However, with the arrival of statistical reconstruction algorithms (32,33) (and the concept of the system matrix), even though it is not possible to determine these effects for each particular detected event, it is possible to calculate and incorporate their probability distributions into the system matrix (e.g. see (34)). Such advanced modeling in turn can result in improvements in image resolution. It has also been suggested (35) that this can improve the noise properties, as also shown (20) in the case

---

6. However, there are other more important motivations for implementation of such combined/simultaneous systems (the interested reader is referred to (30,31) for more details): they include providing the abilities (i) to avoid inaccuracies of registration between functional and anatomic images (e.g. avoiding problems of subject movement and any deformation

of organs in-between scans); (ii) to perform functional MRI (fMRI) and PET in exactly the same environment (e.g. for cross-validation), and (iii) similarly to provide temporal correlation for PET and NMR spectroscopy as a potentially very powerful technique. Furthermore, patient motion may be potentially monitored using MRI, and subsequently incorporated into PET image reconstruction.

of incorporating collimator-detector response modeling in SPECT (see Sec. III-B).

From the above observations, it is evident that improvements in the PET technology as well as reconstruction algorithms will continue to yield further improvements in high-resolution PET imaging. There has been notable activity in this field, in the particular context of small animal PET imaging (see (75) for an elaborate review, including additional considerations), resulting in reconstructed volumetric resolutions reaching ~1microL (e.g. microPET II scanner (76)). As a last note, a very promising ongoing technological development is the use of avalanche photodiodes (APDs) whose compactness compared to bulky photomultiplier tubes (PMTs) offers new opportunities in high resolution imaging (in addition to their high quantum efficiency, internal gain and insensitivity to magnetic fields, as well as the potential of these silicon-based detectors to be ultimately made very cheaply in high volumes,); e.g. see (77,78).

IV. TEMPORAL RESOLUTION

The ability to perform dynamic imaging in nuclear medicine is becoming increasingly important. This is because in many cases, it is the change in the bio-distribution of radiopharmaceuticals within the body that offers the most information about the underlying physiological processes. This in turn brings in the concept of temporal resolution: how frequently (over a period of time) an imaging instrument is able to capture 'acceptable'[7] images of an object in the FoV.

---

7. Compared to spatial resolution, it is more difficult to precisely quantify temporal resolution. This depends on specifying what may or may not be considered as an 'acceptable' image of sufficient quality. The criteria of sufficient image quality are specific to the particular imaging task.

It must be noted that the temporal resolution has a dependence on the reconstruction algorithm being used. For instance, as noted in Sec. III, the use of advanced statistical reconstruction algorithms, e.g. modeling positron range (in PET) or collimator-detector response (in SPECT), can improve image qualities (e.g. both resolution and signal-to-noise ratios), thus improving the temporal resolution. As noted in Sec. II-B, the temporal resolution is also very closely related to the sensitivity of the scanner. In this sense, PET imaging has an intrinsic advantage over SPECT for dynamic studies.

A) Dynamic SPECT

In SPECT (without having an assumptions about image dynamics), it is necessary to perform complete angle tomography via camera rotations for each dynamic frame, which limits how fast each frame may be acquired (an exception to this is stationary multi-pinhole SPECT used in animal imaging, as discussed in Sec. III-A, which does not involve camera rotations, though it involves a limited FoV). Even when using very fast rotation acquisitions (down to even 5 sec per rotation with a three-head camera), the acquisitions at each position will provide very low statistics.

An alternative approach in SPECT is to perform slow camera rotations (e.g. a single rotation for the entire study) while making assumptions about image dynamics. For instance, in fatty acid myocardial viability studies, it has been assumed that the activity $I_j(t)$ of the jth position (voxel) of the heart at time t may be modeled as:

$$I_j(t) = A_j e^{-a_j t} + B_j e^{-b_j t} + C_j \qquad (4)$$

where the abovementioned approach would involve estimating the five kinetic parameters Aj, Bj, Cj, aj and bj, directly from the measured

data (36) (also consult (37) for a list of references using this type of approach).

In (38,39) the authors have instead approached this problem by making no strict assumptions about the functional behaviour of the tracer over time (i.e. unlike Eq. 4) and instead have made the minimal assumption that the activity at each voxel j does not increase with time[8]. While such methods provide less restriction, the problem with not making implicit kinetic model assumptions can be shown in an example: for a typical image slice of size 64x64 reconstructed into 16 dynamic frames from data acquired over 64 projections (each with 64 bins), this last approach requires using 64^2 measurements to estimate 16×64^2 unknowns (i.e. activity of each voxel at each frame), which is highly underestimated. On the other hand, using the direct parameter estimation model above (e.g. Eq. 4 which contains 5 parameters to be estimated for each voxel), 5×64^2 unknowns need to be estimated.

An alternative, more natural approach (37) to dynamic SPECT involves the use of 4D maximum a posteriori (MAP) reconstruction algorithms in which the behaviour of each voxel in time is encouraged to conform to a compartmental model[9]. The interested reader may refer to Ref. (41, p. 9) for an explanation of 4D-MAP image reconstructions[10].

---

8. In Ref. (40), a more flexible scenario is considered in which organ uptake (i.e. increasing activity) is allowed at the beginning.

9. In the mentioned work, the kinetic parameters are updated after every iteration of the reconstruction algorithm.

10. It must be noted, however, that Ref. (41) discusses the different context of 4D reconstruction of cardiac/respiratory-gated data. In such a context, 4D-MAP approaches are used to encourage the behaviour of each voxel to conform to the measured or modeled cardiac/respiratory motion.

B) Dynamic PET

Dynamic PET imaging does not encounter the mentioned complications with dynamic SPECT. A general approach to dynamic PET imaging consists of independently reconstructing tomographic data obtained within each dynamic frame (e.g. (42)). Nevertheless, recent work has indicated that the availability of list-mode acquisition capability in modern PET scanners in which the time-of-detection for each event is also stored (43) can be used to further improve temporal resolution. This is because conventional dynamic PET reconstruction methods assume the activity to be constant within each frame. Instead, new approaches (44,45) make use of temporal basis functions to allow the activity in each voxel to be represented continuously over time. Next, the coefficients of the basis functions are estimated making collective use of the entire dataset and the individual times-of-arrival for each event (this is an example of 4D-PET reconstruction).

Another interesting application of PET is in dynamic-cardiac imaging. As an example, ^{13}N-labeled ammonia ($^{13}NH_3$) can be used for the measurement of myocardial blood flow which makes it possible to measure blood flow at the level of micro-circulation. At the same time, measurement of myocardial wall motion can be used to assess the global function of the heart through the ejection fraction. These tasks can be performed by introduction of dynamic frames each of which are cardiac-gated (which has the additional advantage of reducing cardiac motion artifacts). It is worth noting that in this context, temporal resolution may be further improved by truly 5D (3D+dynamic-1D+gated-1D) reconstruction algorithms which make use of the list-mode data and continuous temporal representation of activities in the voxels, across the frames and the gates (46).

V. ATTENUATION CORRECTION

Photon attenuation refers to the property of emitted radiation to interact with tissue and other materials as it passes through the body. For photon energies encountered in nuclear medicine (68 to 80 keV for ^{201}T1 to 511 keV for positron emitters), photons can undergo photoelectric interactions (though not significant at 511 keV) as well as scattering. Mathematically, the surviving probability of radiation (i.e. not being attenuated) along a path L through an attenuating object can be expressed as:

$$P_L = \exp\left(-\int_L m(\vec{x})d\vec{x} \right) \quad (5)$$

where the parameter μ is referred to as the linear attenuation coefficient, which is an energy-dependent measure of photon attenuation.

The critical observation is that in PET, the path length L represent the line-of-response (LOR) along which the dually-emitted photons travel, and therefore is independent of the point of origin along the LOR, whereas in SPECT, due to its single photon nature, it changes depending on the point of emission. The task of attenuation correction in PET is therefore more straightforward. A number of approaches have been proposed (as reviewed in (47)) most common of which include incorporation of the measured attenuation factors for each LOR as (i) pre-correction factors in the measured data or as (ii) multiplicative factors inside the system matrix of the image reconstruction task.

What we wish to emphasize in this section is that attenuation correction in SPECT is not a limitation, rather it is simply more challenging to address; in the past, due to weak hardware/software implementations (as well as a desire to minimize time and expense costs), attenuation correction has not been widely performed in SPECT. However, the importance of attenuation correction in SPECT is becoming increasingly realized[11] (e.g. (48,49,50)). As such, it has become widely accepted that artifact-free, quantitatively accurate SPECT imaging may only be performed including attenuation correction. Introduction of SPECT/CT scanners has served as a convenient and fast solution to measurement of the transmission data using x-rays (51). However, effects such as respiratory-induced misregistration of the emission and transmission data (52) as well as 'beam-hardening' artifacts caused by the polychromatic nature of CT x-rays (53,54) need to be carefully considered.

In the past, for applications employing attenuation correction in SPECT, the "multiplicative Chang technique" (55) (as well as its iterative versions) had been mostly used; however, these techniques are based on the assumption of uniformly attenuating medium. On the other hand, statistical reconstruction algorithms have a special ability to model (and compensate) for the presence of uniform or non-uniform attenuation in the detection process (e.g. the attenuated projector-backprojector pair as described by Gullberg et al. (56)). With the increasingly realization of the importance (20) and convenience (16,17) of compensation for both the CDR function as well as non-uniform attenuation (particularly using convenient rotation-based projectors as elaborated in Sec. III-B), attenuation compensation statistical

---

11. Since the thickness of tissue varies for different regions of the patient's anatomy, errors introduced by lack of attenuation correction will also vary regionally (e.g. a lesion located deep within the body will produce a more highly attenuated signal compared to a superficial lesion; also, for instance, in myocardial perfusion imaging, soft-tissue attenuation due to the diaphragm or breast tissue can cause false-positive defects).

methods are finally moving towards wide acceptance by the SPECT community.

VI. RANDOM COINCIDENCES IN PET

The technique of coincidence-detection used in PET has a complication (not present in SPECT) in that two gamma rays that are detected/accepted within the same coincidence timing window, may not have originated from the same event. An example of this is shown in Fig. 7 in which an incorrect LOR is assigned to two simultaneous gamma rays whose pairs exit the scanner undetected[12]. Mathematically, the rate of random coincidences along such an LOR connecting two detectors i and j is given by

$$R = 2tS_iS_j \qquad (6)$$

where t is the coincidence timing window, and Si and Sj refer to the singles rates at the two detectors.
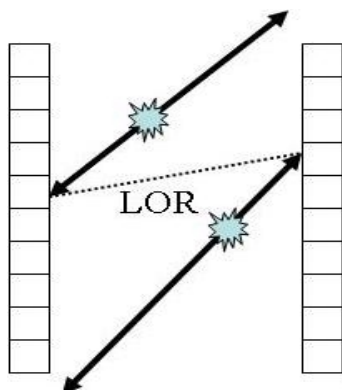

Figure 7: A scenario for the detection of random coincidences in PET.

Correction for random coincidences (randoms) is the subject of ongoing research in PET imaging. In (42) Rahmim et al. have included an elaborate review of relevant techniques (particularly in the context of statistical image reconstruction). The conventional approach has been to subtract a (noisy, Poisson-distributed) estimate of the randoms (obtained using the delayed-coincidence technique) from the measured coincidences. There is, however, two issues with this approach: (1) Even though this approach corrects for randoms on the average, it increases the noise in the data.

(2) Data corrected in this way are no longer Poisson-distributed[13], while most existing statistical image reconstruction algorithms assume Poisson distribution of the data.

Alternatively, to avoid the above two issues, it is possible to follow an approach in which an averaged (i.e. non-noisy) estimate of the random rates along each LOR are included in the image reconstruction task (see (42) for more details). The random rates estimates, required in this approach, can be calculated using: (i) singles measurements at the detectors (57) to calculate the expected randoms contribution according to Eq. 6, or ii) variance reduction (smoothing) of the measured noisy (delayed-coincidence) estimates of randoms (58,59,60).

Defining T and R as the number of true and random coincidences detected in a scan, and using Poisson-statistics arguments (while neglecting scattered events), it can be shown that the SNR in the data is given by

$$SNR = \frac{T}{\sqrt{T + 2R}} \qquad (7)$$

---

12. Alternatively, the other pairs could also have been not detected due to being scattered out of the field-of-view (i.e. attenuated) or simply passed through the scanner undetected (detectors are not 100% efficient).

---

13. A subtraction of Poisson variables results in a variable that is no longer Poisson-distributed (unlike addition).

when using a delayed-coincidence subtraction technique, while it improves (increases) to

$$SNR = \frac{T}{\sqrt{T + R}}$$

(8)

when using the alternative approaches discussed above. Considering equation 8, we note that while in PET random rates are of the same approximate order as the trues rates (R~T), in SPECT random-coincidences do not exist (R=0); however since T(PET)>>T(SPECT), it follows that SNRs are still considerably greater in PET compared to SPECT imaging.

It must further be noted that the discovery of fast (and at the same time high-output) scintillators such as LSO have allowed the coincidence timing window τ to be noticeably reduced (2-4 ns) compared to typical values (~10-12 ns) achieved with conventional BGO scanners (61). Considering Eq. 6, this improvement can be seen to reduce the random rates, and thus to further improve count-rate performance of PET scanners (as a side note: LSO in fact has the potential of exhibiting a timing FWHM resolution of <0.5 ns, which is a very important consideration in time-of-flight PET; see Sec. VII).

Therefore, as a final note in this section, consideration of fast scintillators in PET, as well as careful estimations of random coincidences and their inclusion in appropriate (42) image reconstruction algorithms can result in successful removal of bias in the images while also minimizing degradation/noise-amplification in the PET data.

VII. TIME-OF-FLIGHT DETECTION IN PET

An additional improvement in the quality of PET images may be made making use of the dual nature of emitted gamma rays. Time-of-flight (ToF) PET is based on the observation that by measuring the difference of the arrival times of the 511 keV photons, a PET camera could restrict the position of the positron emission to a subsection of the line segment joining the detector pair. This is shown in figure 8.
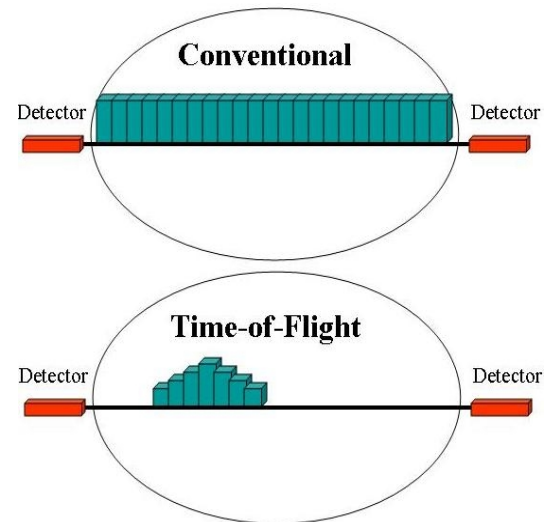

Figure 8: With conventional reconstruction (top) voxels along the LOR are incremented regardless of position along the LOR. With TOF reconstruction (bottom), each voxel is incremented by the probability (as measured by the TOF measurement) that the source originated at that voxel.

It had been known since the early 1980s that PET scanners capable of encoding time-of-flight (TOF) information would potentially reduce the statistical noise variance in PET reconstruction (62,63). However, technological difficulties (slow electronics and the need for fast and at the same time effectively-absorbing scintillators), had limited development of ToF PET until recently. With the continuous improvements in the technology of PET imaging (e.g. faster electronics), and especially since the discovery of the scintillator LSO, time-of-flight PET is now being actively reconsidered (64,61).

ToF PET, especially in whole body scanning, is expected to considerably improve image noise behavior compared to conventional schemes in which ToF information is not incorporated. The reduction factor f in the noise variance for a ToF system capable of a timing resolution of Δt is given by (61):

$$f \approx \frac{2D}{c\Delta t}$$

(9)

where D is the size of the emission source, and c is the speed of light (Ref (65) should be consulted for a more detailed consideration of the effects of random coincidences and scattered events). In fact, optimum Δt values down to ~300ps and ~200ps have been measured for LSO and LaBr3 both of which are very promising ToF scintillators. For a realistic Δt of ~500ps (expected for next-generation LSO-based scanners), the noise variance improvements will correspond to factors of ~4.7 in whole-body (D~35 cm) and ~2.7 in brain (D~20 cm) imaging.

VIII. DUAL ISOTOPE SPECT IMAGING

Simultaneous dual isotope imaging using SPECT is an area of increasing interest. The dual-isotope approach can not be performed in PET imaging due to all its radiotracers being of the same energy level (511keV), whereas multiple energy windows can be used in SPECT for simultaneous imaging of radiotracers of different energies.

Examples of this include: (i) ^{99m}Tc(140keV) sestamibi stress and ^{201}Tl(75keV/167keV) rest myocardial perfusion imaging, and (ii) simultaneous use of a ^{99m}Tc(140keV) labeled perfusion agent and an ^{123}I(159keV) labeled neurotransmitter agent (with potential applications in diagnosis of neurodegenerative

diseases, e.g. Parkinson's, Huntington's and Alzheimer's diseases).

The use of simultaneous acquisition reduces acquisition times and therefore patient discomfort and image artifacts due to patient motion. Another significant advantage is that the resulting images from the different isotopes are perfectly registered in space and time.

A complication with dual-isotope imaging is the presence of crosstalk between the multiple energy windows. In the case of, for instance, imaging with ^{99m}Tc(140keV) and ^{201}Tl(75keV/167keV), the lower-energy ^{201}Tl energy window is contaminated by ^{99m}Tc photons scattered in the patient or collimator (referred to as down-scatter) as well as Pb x-rays generated by both scattered and unscattered ^{99m}Tc photons in the collimator. In addition, the Tc data are also contaminated by scattered (~135keV) and unscattered (167 keV) ^{201}Tl photons.

To address the above difficulties, current research has focused on optimization of multiple energy-window acquisition parameters (66,67) as well as modeling of crosstalk effects (i.e. down-scatter and collimator x-ray generation) in the reconstruction task (68). Combination of these methods as well as detailed clinical evaluation are still required in order to make dual-isotope SPECT imaging an acceptable clinical protocol.

IX. OTHER CORRECTIONS

In order to produce fully quantitative data, three other corrections need to be considered. The reader is referred elsewhere for elaborate reviews of these topics; here we briefly compare their applications in PET vs. SPECT.

A) Scatter Correction
Scatter correction is one of the most important and at the same time most difficult corrections in

nuclear medicine imaging. Scattered events can constitute 30-50% of all events in SPECT, 10-20% in 2D-PET and 40-60% in 3D-PET. The difficulty in scatter compensation is given by the fact that in order to truly estimate the number of scattered events along each projection, the emission image needs to be known, which is the very aim of the reconstruction task! The reader is referred to (69) for a thorough review of the various approaches.

An approach of increasing interest is the use of fast analytic (70) or Monte Carlo (71) scatter calculations inside iterative reconstruction algorithms, such that the scatter estimate is updated at every step. However, it must be noted that due to the comparatively much larger sizes of data in PET, most of the research performed in this field is related to SPECT imaging (as an exception see (72) for an application in PET). Another example of this iterative application (68) was discussed in the estimation of down-scatter in dual-isotope imaging (see Sec. VIII).

B) Correction for the Partial Volume Effect

The partial volume effect (PVE) arises due to the limited resolution in nuclear medicine imaging (and is relevant for "small" regions with dimensions smaller than around 2 times the FWHM of the scanner resolution). It has been shown to result in large biases in the estimates of regional radioactivity concentrations. The reader is referred to (73) for an elaborate review of this topic. The methods developed in this area are equally applicable in both PET and SPECT imaging, and require, for best performance, access to anatomical images (e.g. MRI) of the subjects.

C) Motion Compensation

The majority of motion-compensation methods (image-based and projection-based) are equally

applicable in both PET and SPECT. These have been reviewed, for rigid, cardiac and respiratory motions, in Ref. (41). There are, however, two potential differences between the two modalities in the context of motion compensation:

(1) In SPECT, there exists a correlation between projection angle and time (therefore motion); this time-dependence may be potentially used in the motion compensation task (e.g. (74)).

(2) The enormous size of PET data can cause difficulties for demanding motion compensation methods. Subsequently, accurate and at the same time fast methods are needed in PET (see (41) for details).

X. CONCLUSION

The present work has attempted to summarize important themes of ongoing hardware and software advancements for the two major imaging modalities in nuclear medicine: PET and SPECT.

In the context of PET imaging, the coincidence-detection method is viewed as a very powerful method, considerably enhancing sensitivity (Sec. II-B) and dynamic-imaging (Sec. IV) capabilities of PET. Furthermore, (i) use of very short half-life tracers (e.g. Rubidium) injected at very high activities (Sec. II-C), as well as (ii) the introduction of increasingly fast scintillators technology (particularly for LSO), which in turn has allowed reduction of random coincidences (Sec. VI) and introduced the possibility of time-of-flight PET (Sec. VII) are expected to further contribute to high-sensitivity imaging capabilities of PET.

Improvements in PET technology (e.g. detector design), modeling of finite resolution effects in PET image reconstruction, as well as the potential of applying magnetic fields (expected to reduce positron range for high-energy positron-emitting radio-nuclides) are also seen as

areas of ongoing research attempting to improve resolution limitations in PET.

In SPECT, the use of specialized collimators (e.g. slant-hole) are seen as techniques improving sensitivity without degrading image resolution. Furthermore, the pinhole SPECT technology is seen as an area of intense recent interest, particularly due to its ability to enhance resolution capabilities in SPECT (to sub-millimeter range) and to the possibility of stationary SPECT small animal imaging.

Incorporation of non-uniform attenuation in SPECT (Sec. V) as well as collimator-detector response (Sec. III-B) and scatter (Sec. IX-A) modeling into statistical, iterative image reconstruction algorithms was also seen as an area of considerable potential towards artifact-free, quantitative SPECT imaging. Various issues related to temporal resolution (and dynamic imaging capabilities) in SPECT and PET were also discussed. In particular, it was seen that use of suitable (4D and 5D) reconstruction algorithms could further enhance temporal resolution capabilities in these modalities.

Finally, it should be stressed that existing PET and SPECT scanners in the field can (much) benefit from improvements in image-reconstruction software (as discussed in this review), and in the case of SPECT imaging, from the potential of dual-isotope imaging (Sec. VIII) as well as the use of specialized collimators (Secs. II-A and III-A).

XI. REFERENCES

1. Ollinger JM, Fessler JA. Positron emission tomography. IEEE Sig Proc Mag. 1997; 14: 43-55.

2. Segall, G. Assessment of myocardial viability by positron emission tomography. Nucl Med Communications. 2002; 23: 323-330.

3. Lodge MA, Webb S, Flower MA, Binnie DM. A prototype rotating slat collimator for single photon emission computed tomography. IEEE Trans Med Imag. 1996; 15: 500-511.

4. Tsui BM, Gullberg GT. The geometric transfer function for cone and fan beam collimators. Phys Med Biol. 1990; 35: 81-93.

5. Clack R, Christian PE, Defrise M, Welch AE. Image reconstruction for a novel SPECT system with rotating slant-hole collimators. IEEE Med Imag Conf. 1994; 4: 1948-1952.

6. Wagner J-M, Noo F, Clackdoyle R. Exact inversion of the exponential x-ray transform for rotating slant-hole (RSH) SPECT. Phys Med Biol. 2002; 47: 2713-2726.

7. Strother SC, Casey ME, Hoffman EJ. Measuring PET scanner sensitivity: relating countrates to image signal-to-noise ratios using noise equivalents counts. IEEE Trans Nucl Sci. 1990; 2: 783-788.

8. Stearns CW. Estimating an acquisition-specific NEC curve for PET acquisitions. IEEE Nucl Sci Symp Conf Rec. 2003; 4: 2578-2580.

9. Stearns CW. NEC and local image noise in PET imaging. IEEE Nucl. Sci. Symp. Conf. Rec. 2004; 5: 3106-3108.

10. Jadvar H, Strauss HW, Segall GM. SPECT and PET in the evaluation of coronary artery disease. RadioGraphics. 1999; 19: 915-926.

11. McElroy DP, McDonald LR, Beekman FJ, Wang Y, Patt BE, Iwanczyc JS *et al*. Performance evaluation of SPECT: a high resolution desktop pinhole SPECT system for

imaging small animals. IEEE Trans Nucl Sci. 2002; 49: 2139-2147.

12. Schramm NU, Ebel G, Engeland U, Schurrat T, Behe M, Behr TM. High-Resolution SPECT Using Multipinhole Collimation. IEEE Trans Nucl Sci. 2003; 50: 315-320.

13. Beekman FJ, Vastenhouw B. Design and simulation of a high-resolution stationary SPECT system for small animals. Phys Med Biol. 2004; 49: 4579-4592.

14. Du Y, Frey EC, Wang WT, Tocharoenchai C, Baird WH, *et al*. Combination of MCNP and SimSET for Monte Carlo simulation of SPECT with medium- and high-energy photons. IEEE Trans Nucl Sci. 2002; 49: 668-674.

15. Frey EC, Tsui BMW. Collimator-detector response compensation in SPECT In: Zaidi H. Quantitative analysis in nuclear medicine imaging". New York: Springer. 2006.

16. McCarthy AW, Miller MI. Maximum-likelihood SPECT in clinical computation times using mesh-connected parallel computers. IEEE Trans Med Imag. 1991; 10: 426-436.

17. Zeng GL, Gullberg GT. Frequency domain implementation of the three-dimensional geometric point source correction in SPECT imaging. IEEE Trans Nucl Sci. 1992; 39: 1444-1453.

18. Kohli V, King MA, Glick SJ, Pan TS. Comparison of frequency-distance relationship and Gaussian-diffusion based methods of compensation for distance-dependent spatial resolution in SPECT imaging. Phys Med Biol. 1998; 43: 1025-1037.

19. King MA, Pan TS, Luo DS. An investigation of aliasing with Gaussian-diffusion modeling of SPECT system spatial resolution. IEEE Trans Nucl Sci. 1997; 44: 1375-1380.

20. Tsui BMW, Frey EC, Zhao XD, Lalush DS, Jahnston ER, *et al.* The importance and implementation of accurate three-dimensional compensation methods for quantitative SPECT. Phys Med Biol. 1994; 39: 509-530.

21. Kohli V, King MA, Pan TS, Glik SG. Compensation for distance-dependent resolution in cardiac-perfusion SPECT: impact on uniformity of wall counts and wall thickness. IEEE Trans Nucl Sci. 1998; 45: 1104-1110.

22. Sankaran S, Frey EC, Gilland KL, Tsui BMW. Optimum compensation method and filter cutoff frequency in myocardial SPECT: A human observer study. J Nucl Med. 2002; 43: 432-438.

23. Frey EC, Gilland KL, Tsui BMW. Application of task-based measures of image quality to optimization and evaluation of three-dimensional reconstruction-based compensation methods in myocardial perfusion SPECT. IEEE Trans Med Imaging. 2002; 21: 1040-1050.

24. Narayanan MV, King MA, Pretorius PH, Dahlberg ST, Spencer F, Simon E, *et al.* Human-observer receiver-operating-characteristic evaluation of attenuation, scatter, and resolution compensation strategies for Tc-99m myocardial perfusion imaging. J Nucl Med. 2003; 1725-1734.

25. Gifford HC, King MA, Wells RG, Hawkins WG, Narayanan MV, Pretorius PH. LROC analysis of detector-response compensation in SPECT. IEEE Trans Med Imaging. 2000; 19: 463-473.

26. Mumcuoglu EU, Leahy RM, Cherry SR, Hoffman E. Accurate geometric and physical response modelling for statistical image reconstruction in high resolution PET. IEEE Nucl Sci Symp Conf Record. 1996; 3: 1569-1573.

27. Levin CS, Hoffman EJ. Calculation of positron range and its effect on the fundamental limit of positron emission tomography system spatial resolution. Phys Med Biol. 1999; 44: 781-799.

28. Raylman RR, Hammer BE, Christensen NL. Combined MRI-PET Scanner: A Monter Carlo Evaluation of the Improvements in PET Resolution Due to the Effects of a Static Homogeneous Magnetic Field. IEEE Trans Nucl Sci 1996; 43: 2406-2412.

29. Winwar A, Vosberg H, Herzog H, Halling H, Weber S, Muller-Gartner HW. 4.5 Tesla magnetic field reduces range of high-energy positrons – potential implications for positron emission tomography. IEEE Trans Nucl Sci. 1997; 44: 184-189.

30. Shao Y. Cherry SR, Farahani K, Slates R, Silverman RW, Meadors K, Bowery A, Siegel S. Development of a PET detector system compatible with MRI/NMR systems. IEEE Trans Nucl Sci. 1997; 44: 1167-1171.

31. Mackewn JE, Strul D, Hallett WA, Halsted P, Page RA, Keevil SF, Williams SCR, Cherry SR, Marsden PK. Design and development of an MR-compatible PET scanner for imaging small animals. IEEE Trans Nucl Sci. 2005; 52: 1376-1380.

32. Shepp LA, Vardi Y. Maximum likelihood reconstruction for emission tomography. IEEE Trans Med Imag. 1982; 1: 113-123.

33. Lange K, Carson R. EM reconstruction for emission and transmission tomography. J Comput Assist Tomogr. 1984; 8: 306-312.

34. Reader AJ, Ally S, Bakatselos F, Manavaki R. One-pass list-mode EM algorithm for high-resolution 3-D PET image reconstruction into large arrays. IEEE Trans Nucl Sci. 2002; 49: 693-699.

35. Rahmim A, Cheng JC, Sossi V. Improved noise propagation in statistical image reconstruction with resolution modeling. IEEE Med Imag Conf Records. 2005.

36. Limber MA, Limber MN, Celler A, Barney JS, Borwein JM. Direct reconstruction of functional parameters for dynamic SPECT. IEEE Trans Nucl Sci. 1995; 42: 1249-1256.

37. Kadrmas DJ, Gullberg GT. 4D maximum *a posteriori* reconstruction in dynamic SPECT using a compartmental model-based prior. Phys Med Biol. 2001; 46: 1553-1574.

38. Farncombe T, Celler A, Noll D, Maight J, Harrop R. Dynamic SPECT imaging using a single camera rotation (dSPECT). IEEE Trans Nucl Sci. 1999; 46: 1055-1061.

39. Bauschke HH, Dominikus N, Celler A. An EM Algorithm for dynamic SPECT. IEEE Trans Med Imag. 1999; 18: 252-261.

40. Farncombe T, Celler A, Bever C, Noll D, Maeght, Harrop R. The incorporation of organ uptake into dynamic SPECT (dSPECT) image reconstruction. IEEE Trans Nucl Sci. 2001; 48: 3-9.

41. Rahmim A. Advanced motion correction methods in PET. Iran J Nucl Med. 2005; 13 (24): 1-17.

42. Rahmim A, Cheng JC, Blinder S, Camborde ML, Sossi V. Statistical dynamic image reconstruction in state-of-the-art high resolution PET. Phys Med Biol. 2005; 50:4887-4912.

43. Rahmim A, Statistical list-mode image reconstruction and motion compensation techniques in high-resolution positron emission tomography (PET). PhD thesis. Vancouver, Canada. 2005.

44. Nichols TE, Qi J, Asma E, Leahy RM. Spatiotemporal Reconstruction of list-mode PET data. IEEE Trans Med Imag. 2002; 21: 396-404.

45. Verhaeghe J *et al.* ML Reconstruction from Dynamic List-Mode PET Data Using

Temporal Splines. IEEE Med. Imag. Conf. Records. 2004; 5: 3146-3150.

46. Verhaeghe J. Five dimensional reconstruction on tensor product splines in cardiac PET. Proc 8th Intern Meeting on Fully 3D Image Recon in Radiol and Nucl Med. 2005; 167-171.

47. Zaidi H, Hasegawa BH. Attenuation correction strategies in emission tomography In: Zaidi H. Quantitative analysis in nuclear medicine imaging. New York: Springer. 2006.

48. Wachers FJ. Should SPET attenuation correction be more widely employed in routine clinical practice? Eur J Nucl Med. 2002; 29: 412-415.

49. Ficaro EP. Should SPET attenuation correction be more widely employed in routine clinical practice? Eur J Nucl Med. 2002; 29: 409-412.

50. Hendel RC, Corbett JR, Cullom SJ. The value and practive of attenuation correction for myocardial persusion SPECT imaging: a joint position statement from the American Society of Nuclear Cardiology and the Society of Nuclear Medicine. J Nucl Cardiol. 2002; 9: 135-143.

51. Blankespoor SC, Xu X, Kaiki K. Attenuation correction of SPECT using X-ray CT on an emission-transmission CT system: myocardial perfusion assessment. IEEE Trans Nucl Sci. 1996; 43: 2263-2274.

52. Osman MM, Cohade C, Nakamoto Y, Wahl RL. Respiratory motion artifacts on PET emission images obtained using CT attenuation correction on PET-CT. Eur J Nucl Med Mol Imaging. 2003; 30: 603-606.

53. Hsieh J, Molthen RC, Dawson CA, Johnson RH. An iterative approach to the beam hardening correction in cone beam CT. Med Phys. 2000; 27: 23-29.

54. Kachelriess M, Kalender WA. Improving PET/CT Attenuation Correction with Iterative CT Beam Hardening Correction. IEEE Med Imag Conf Records. 2005.

55. Chang LT. A method for attenuation correction in radionuclide computed tomography. IEEE Trans Nucl Sci 1978: 638-643.

56. Gullberg GT, Huesman RH, Malko JA, Pelc NJ, Budinger TF. An attenuated projector-backprojector for iterative SPECT reconstruction. Phys Med Biol. 1985; 30: 799-816.

57. Rokitta O, Casey M, Wienhard K, Pictrzyk U. Random correction for positron emission tomography using singles count rates. IEEE Nucl Sci Symp Conf Record. 2000; 3: 17/37 - 17/40.

58. Casey ME, Hoffman EJ. Quantitation in positron emission tomography: 7. A technique to reduce noise in accidental concidence meansurements and coincidence efficinecy calibration. J Comput Assist Tomogr. 1986: 10:845-850.

59. Mumcuoglu EU, Leahy RM, Cherry SR. Baysian reconstruction of PET images: methodology and performance analysis. Phys Med Biol. 1996; 41:1777-1807.

60. Badawi RD, Miller MP, Bailey DL, Marsden PK. Randoms variance-reduction in 3D-PET. Phys Med Biol. 1999; 44:941-954.

61. Moses WW. Time of flight in PET revisited. IEEE Trans Nucl Sci. 2003; 50: 1325-1330.

62. Snyder DL, Thomas LJ, Ter-Pogossian MM. A mathematical model for positron-emission tomography systems having time-of-flight measurements. IEEE Trans Nucl Sci. 1981; 28: 3575-3583.

63. Tomitani T. Image reconstruction and noise evaluation in photon time-of-flight assisted positron emission tomography. IEEE Trans

Nucl Sci. 1981; 28: 4582-4589.

64. Moses WW, Derenzo SE. Prospects for time-of-flight PET using LSO Scintillators. IEEE Trans Nucl Sci. 1999; 46: 474-478.

65. Conti M. Effect of Randoms on Signal-to-noise-ratio in TOF PET. IEEE Med Imag Conf. Records. 2005.

66. Wang WT, Tsui BMW, Lalush DS, Tocharoenchai C, Frey EC. Optimization of acquisition parameters for simultaneous ^{201}Tl and ^{99m}Tc dual-isotope myocardial imaging. IEEE Trans Nucl Sci. 2005; 52: 1227-1235.

67. Du Y, Frey EC, Wang WT, Tsui BMW. Optimization of acquisition energy windows in simultaneous ^{99m}Tc/^{123}I brain SPECT. IEEE Trans Nucl Sci. 2003; 50: 1556-1561.

68. Song X, Frey EC, Wang WT, Du Y, Tsui BMW. Validation and evaluation of model-based crosstalk compensation method in simultaneous ^{99m}Tc stress and ^{201}Tl rest myocardial perfusion SPECT. IEEE Trans Nucl Sci. 2004; 51: 72 -79.

69. Zaidi H, Koral KF. Scatter correction strategies in emission tomography. In: Zaidi H. Quantitative analysis in nuclear medicine imaging. New York: Springer. 2006.

70. Frey EC, Tsui BMW. A fast projector-backprojector pair modeling the asymmetric, spatially varying scatter response function for scatter compensation in SPECT imaging. IEEE Trans Nucl Sci. 1993; 40: 1192-1197.

71. Beekman FJ, de Jong HW, van Geloven S. Efficient fully 3-D iterative SPECT reconstruction with Monte Carlo-based scatter compensation. IEEE Trans Med Imaging. 2002; 21: 867-877.

72. Werling A, Bublitz O, Doll J. Adam LE, Brix G. Fast implementation of the single scatter simulation algorithm and its use in iterative image reconstruction of PET data. Phys Med Biol. 2002; 47: 2947-2960.

73. Rousset OG, Zaidi H. Correction for partial volume effects in emission tomography In: Zaidi H. Quantitative analysis in nuclear medicine imaging. New York: Springer. 2006.

74. Lu W. Mackie TR. Tomographic motion detection and correction directly in sinogram space. Phys Med Biol. 2002; 47: 1267-1284.

75. Chatziioannou AF. Molecular imaging of small animals with dedicated PET tomographs. Eur J. Nucl Med. 2002; 29: 98-114.

76. Yang Y, Tai Y-C, Siegel S, Newport DF, Bai B, Quanzheng L, Leahy RM, Cherry SR. Optimization and performance evaluation of the microPET II scanner for *in vivo* small-animal imaging. Phys Med Biol. 2004; 49: 2527-2545.

77. Pichler BJ, Swann BK, Rochelle J, Nutt RE, Cherry SR, Siegel SB. Lutetium oxyorthosilicate block detector readout by avalanche photodioide arraysfor high resolution animal PET. Phys Med Biol. 2004; 49: 4305-4319.

78. Shah KS, Grazioso R, Farrell R, Glodo J, McClish M, Entine G, Dokhale P, Cherry SR. Position sensitive APDs for small animal PET imaging. IEEE Trans Nucl Sci. 2004; 51: 91-95.